Bioactive Materials 10 (2022) 222–235

Contents lists available at ScienceDirect

Bioactive Materials

journal homepage: www.keaipublishing.com/en/journals/bioactive-materials

Effect of minor amounts of β-calcium pyrophosphate and hydroxyapatite on the physico-chemical properties and osteoclastic resorption of β-tricalcium phosphate cylinders

B. Le Gars Santoni [a,b], L. Niggli [a], S. Dolder [c], O. Loeffel [d], G.A. Sblendorio [e], R. Heuberger [d], Y. Maazouz [a], C. Stähli [a], N. Döbelin [a], P. Bowen [e], W. Hofstetter [c], M. Bohner [a,*]

[a] RMS Foundation, Bioceramics and Biocompatibility Group, Bischmattstrasse 12, CH-2544, Bettlach, Switzerland
[b] University of Bern, Graduate School for Cellular and Biomedical Sciences, Mittelstrasse 43, CH-3012, Bern, Switzerland
[c] University of Bern, Department for BioMedical Research (DBMR), Murtenstrasse 35, CH-3008, Bern, Switzerland
[d] RMS Foundation, Materials Group, Bischmattstrasse 12, CH-2544, Bettlach, Switzerland
[e] EPFL, Ecole Polytechnique Fédérale de Lausanne, Construction Materials Laboratory, Station 12, CH-1015, Lausanne, Switzerland

ARTICLE INFO

Keywords:
Bioceramics
Calcium phosphate
β-Tricalcium phosphate
β-Calcium pyrophosphate
Hydroxyapatite
Osteoclastic resorption

ABSTRACT

β-Tricalcium Phosphate (β-TCP), one of the most used bone graft substitutes, may contain up to 5 wt% foreign phase according to standards. Typical foreign phases include β-calcium pyrophosphate (β-CPP) and hydroxyapatite (HA). Currently, the effect of small amounts of impurities on β-TCP resorption is unknown. This is surprising since pyrophosphate is a very potent osteoclast inhibitor. The main aim of this study was to assess the effect of small β-CPP fractions (<1 wt%) on the in vitro osteoclastic resorption of β-TCP. A minor aim was to examine the effect of β-CPP and HA impurities on the physico-chemical properties of β-TCP powders and sintered cylinders. Twenty-six batches of β-TCP powder were produced with a Ca/P molar ratio varying between 1.440 and 1.550. Fifteen were further processed to obtain dense and polished β-TCP cylinders. Finally, six of them, with a Ca/P molar ratio varying between 1.496 (1 wt% β-CPP) and 1.502 (1 wt% HA), were incubated in the presence of osteoclasts. Resorption was quantified by white-light interferometry. Osteoclastic resorption was significantly inhibited by β-CPP fraction in a linear manner. The presence of 1% β-CPP reduced β-TCP resorption by 40%, which underlines the importance of controlling β-CPP content when assessing β-TCP biological performance.

1. Introduction

Every year, millions of patients [1,2] receive bone grafts to fill in or replace bone defects arising from complications of tumours, infections or trauma [3]. To date, the gold standard is still the use of autografts, which come from the patient's own body [4]. The main disadvantages of such grafts are their limited supply and their surgical procedure, which is costly [5,6] and associated with morbidity [7,8]. An alternative consists of using bone grafts originating from either animals (xenografts) [9] or humans (allografts) [10]; however, there is a risk of disease transmission [11] and ethical concerns [12]. Therefore, interest has shifted towards synthetic bone grafts to overcome the disadvantages of biological bone grafts mentioned above.

Synthetic bone grafts are made of various materials, i.e. metals, polymers and ceramics [13,14], but calcium phosphates (CaP) have received particular attention because of their chemical similarity to the mineral part of natural bone and their attractive physico-chemical and biological properties. Among these, beta-tricalcium phosphate (β-TCP; $Ca_3(PO_4)_2$; Ca/P = 1.500) is one of the most used CaP due to its cell-mediated resorption [15,16]. Moreover, after its resorption, β-TCP is replaced by new bone [17,18], demonstrating its osteotransductive [19] and even osteoinductive [19] abilities. For these reasons, β-TCP has been intensively studied.

ISO standard 13175-3:2012 [20] defines "phase pure" β-TCP as a β-TCP containing up to 5 wt% of foreign CaP phases, i.e. β-calcium pyrophosphate (β-CPP; $Ca_2P_2O_7$; Ca/P = 1.000) or hydroxyapatite (HA; $Ca_5(PO_4)_3OH$; Ca/P = 1.667). These foreign CaP phases have physico-chemical and biological properties, which differ from those of

Peer review under responsibility of KeAi Communications Co., Ltd.
* Corresponding author. RMS Foundation, Bischmattstrasse 12, CH-2544 Bettlach, Switzerland.
E-mail address: marc.bohner@rms-foundation.ch (M. Bohner).

https://doi.org/10.1016/j.bioactmat.2021.09.003
Received 16 June 2021; Received in revised form 2 September 2021; Accepted 2 September 2021
Available online 23 September 2021

β-TCP. For instance, at pH 7.4, β-TCP is more soluble than β-CPP and HA [21,22]. Biologically, β-CPP is poorly resorbable and inhibits osteoclastic resorption [23,24], whereas HA is non-resorbable [23,25], which could mean that β-TCP resorption would decrease with minor amounts of β-CPP and HA. Importantly, these secondary phases can also affect β-TCP properties. For example, contrary to HA, β-CPP is known to reduce β-TCP densification at constant sintering temperature ("sinterability") [26,27]. For the osteoclastic resorption, Yamada et al. [28] and Bouler et al. [29] specified that the decrease of the β-TCP/HA ratio in biphasic calcium phosphates (BCP) decreased its resorption rate. However, these studies considered HA contents above 5 wt% and did not explore if smaller amounts could affect the resorption of β-TCP. In addition, to the best of our knowledge, no studies to date have investigated the effect of β-CPP on the osteoclastic resorption of β-TCP. Therefore, the aim and novelty of this study was to assess the effect of slight deviations from the 1.500 Ca/P molar ratio or, in other words, the content of secondary phases (below 5 wt% of β-CPP and HA) on the osteoclastic resorption of "phase pure β-TCP" cylinders. For this purpose, cylinders were manufactured from β-TCP powders with various Ca/P molar ratios. Since the surface topography and chemistry of calcium phosphate materials may also affect osteoclastic resorption [30,31], it was important to control these parameters on the surface of the cylinders during the manufacturing process. Sinterability of the cylinders was evaluated by their grain sizes and their relative densities. Their ability to be resorbed by osteoclasts was observed by scanning electron microscopy (SEM) and measured by white light interferometry and inductively coupled plasma mass spectrometry (ICP-MS).

2. Materials and methods

2.1. Synthesis of β-TCP powders

The β-TCP powders were obtained by thermal conversion (1 h at 850 °C) of calcium deficient hydroxyapatite (CDHA) $Ca_9(HPO_4)(PO_4)_5(OH)$ [26,32,33]. CDHA powders were produced by aqueous precipitation using high purity calcium nitrate (Art N∘102123, Batch N∘B1371623, Merck) and ammonium phosphate (Art N∘5596.1, Batch N∘138269744, Carl Roth) chemicals, according to the procedure described by Le Gars Santoni et al. [34]. A total of 26 different β-TCP powders with varying Ca/P molar ratios were obtained (Table 1). The detailed characterization of these powders was published separately and can be found in Ref. [34].

2.2. Fabrication of β-TCP cylinders

Among the 26 synthesis/batches of β-TCP powder, 15 were selected for the fabrication of cylinders (Table 1). Shaping of β-TCP cylinders was made according to the slip-casting procedure described by Descamps et al. and Gallo et al. [33,35]. β-TCP powders were ball-milled (2 h, in an aqueous solution) to destroy the agglomerates formed during the calcination procedure. Then, the powders were filtered, dried (70 °C) and dispersed with a solution of Darvan C-N (ammonium polymethacrylate, R.T. Vanderbilt Co, USA), with 1.0 wt% of powder content. Finally, the dispersed powders (slurries) were homogenised in a ball-mill for 30 min and then slip cast into a 96 polystyrene well-plate cut at both sides (Art N°3628, Batch N°16117017, Costar®, Corning Incorporated, USA) placed on a gypsum block. After drying and demoulding, dense cylinders were obtained by sintering of the β-TCP green bodies at 1100 °C for 3 h. Finally, one side of β-TCP cylinders was grinded with various SiC papers, polished with diamond suspensions (down to 0.25 μm), and finally polished with a silica suspension (0.2 μm). Polished β-TCP cylinders were then cleaned by ultrasonication (twice 5 min in acetone and once 5 min in ethanol).

Table 1
Factors, levels, responses and sample sizes analysed for CDHA and β-TCP batches. 26 powders were produced, but only 15 powders were used to produce dense β-TCP cylinders.

Factors			Levels	Responses		
				SSA	Grain Size	Relative density
Powders	CDHA	Ca/P molar ratio (bulk)	26	$n = 26$	–	–
	β-TCP	Ca/P molar ratio (bulk)	26	$n = 26$	–	–
Cylinders	β-TCP	Ca/P molar ratio (bulk)	15	–	$n = 15$	$n = 15$

2.3. Characterization of β-TCP powders and cylinders

Specific surface area (SSA) of the particles was determined via nitrogen adsorption using the BET method (Gemini 2360, Micromeritics, USA). Specifically, before the measurements, powders were pre-dried at 130 °C for 2 h under nitrogen flow. Measurements were done in triplicate for all CDHA ($n = 26$; Table 1) and β-TCP powders ($n = 26$; Table 1).

Crystalline compositions of powders/cylinders or in other words their Ca/P molar ratio were determined by X-ray diffraction between 8° and 100° 2θ on a Bruker D8 Advance diffractometer (Bruker AXS GmbH, Germany). Briefly, the XRD patterns were acquired digitally using Ni-filtered Cu Kα radiation (wavelength: 1.540598 Å) and analysed by Rietveld refinement using BGMN software version 4.2.22 [36] and Profex user interface (Version 4.0.2 [37]). Measurements were done in triplicates and importantly, a specific thermal treatment was used as described in ISO 13779-3:2018 (15 h at 1000 °C followed by 15 h at 840 °C [38]).

Elemental impurities in β-TCP powders/cylinders was analysed via inductively coupled plasma mass spectrometry (ICP-MS; Agilent 7700x, Agilent Technologies, USA) as described by *Gallo* et al. [35]. In short, ^{44}Ca and ^{31}P isotopes were calibrated from a certified custom-made CaP standard solution (500:250 ppm Ca:P, Inorganic Ventures, USA). All the other 43 elements such as ^{23}Na, ^{25}Mg, ^{39}K, ^{56}Fe, ^{65}Cu and ^{88}Sr (Zr, Si, Ti, Ge, Mo, W not included) were calibrated with a certified multi element standard (71A, 10 ppm, Inorganic Ventures, USA). Calibration drifts were continuously corrected according to an internal standard solution (1 ppb In, 1 ppb Sc, Inorganic Ventures, USA) measured along with each sample. Ca and P drifts were also corrected by repeated measurement of the CaP standard.

Grain sizes on sintered cylinders were analysed by morphometric analysis of images obtained under a SEM (EVO MA 25, Zeiss, Germany) with backscattered electrons (BSE) detector. Namely, 3 cylinders were investigated for each batch of β-TCP and 4 images per cylinders were acquired. On each image, 250 grain diameters were analysed with ImageJ/Fiji shareware [39], leading to a total of 3000 grain diameters measured for each batch of β-TCP. Importantly, no difference of grain size was observed when looking at the surface of the cylinders and the surface of polished and etched cylinders.

Relative densities of β-TCP cylinders were determined via the Archimedes method in isopropanol. For each batch of β-TCP, measurements were done in triplicate. Densities were expressed relatively to the theoretical β-TCP density measured by X-ray diffraction.

Surface chemistry of the β-TCP cylinders was analysed by X-ray photoelectron spectroscopy (XPS), using an Axis Nova instrument (Kratos Analytical Ltd, UK). The spectra were analysed using CasaXPS software (V2.3.14, Casa Software Ltd., UK).

2.4. Cell culture experiments

Osteoclasts were derived from primary cells following the procedure described by Gallo et al. [35]. Briefly, bone marrow cells (BMC) were obtained from femora and tibiae of 6 weeks old C57Bl/6J mice and cultured for 24 h in α-minimum essential media (α-MEM, Art. N°12000, GIBCO® BRL Life Technologies, Switzerland) supplemented with 10%

fetal bovine serum (FBS, Art. N°F7524, Batch. N°099K3395, Sigma-Aldrich, Switzerland), 1% penicillin/streptomycin (P/S, Art. N°15140, GIBCO BRL Life Technologies, Switzerland) and 30 ng/mL macrophage colony-stimulating factor (M-CSF, Art. N°FDP-3005, Chiron, USA). The non-adherent osteoclast progenitor cells (OPC) were collected, and re-suspended in cell culture medium (α-MEM) with 30 ng/mL of M-CSF and 20 ng/mL of receptor activator of nuclear factor κ-B ligand (recombinant human RANKL, Art. N°310-01, PeproTech, UK). Mature osteoclasts were obtained after 5 days. In the meantime, pure β-TCP cylinders were sterilized by dry heat (180 °C for 6 h) and placed into 96-well plates. The β-TCP cylinders, with the polished surface on top were coated with 150 μL per well of 30% FBS in cell culture medium and incubated for 48 h (37 °C, humidified atmosphere, 5% CO_2). Coating medium was removed after incubation. At day 5, mature osteoclasts were re-suspended in cell culture medium and seeded onto the β-TCP cylinders. Each well containing β-TCP cylinders was filled with 25 μL of cell suspension and 125 μL of medium supplemented with 30 ng/mL M-CSF, 15 mM HCl (37% fuming, Art. N° 317, Merck, Germany) and 20 ng/mL RANKL.

Macrophages were differentiated from OPC in culture media supplemented with M-CSF (30 ng/mL), but without RANKL.

Cell culture experiments were conducted in sextuplicate ($n = 6$) on 6 different batches of β-TCP (CaP1-CaP6) with Ca/P molar ratios close to 1.500 (Table 2). Specifically, each cell culture experiment consisted of placing all β-TCP cylinders in contact for 24 h with the cell culture medium containing no cells (NC), macrophages (MA) and osteoclasts (OC).

OC were assessed by staining for the marker enzyme Tartrate Resistant Acid Phosphatase (TRAP). For this purpose, the cells were washed with PBS, fixed in 4% paraformaldehyde (Art. No. 818715, Merck, Germany)/PBS, rinsed 3 times with demineralized H_2O and stained with a TRAP staining kit (Art. No. 387A, Sigma-Aldrich, Switzerland).

TRAP activity was quantified in the cell lysates by the conversion of *p*-nitrophenyl phosphate (*p*-NPP, Art. No. N3254, Sigma, Switzerland) to *p*-nitrophenol in the presence of sodium tartrate/sodium acetate. The reaction was stopped with NaOH and absorbance was measured at 405 nm (reference wavelength 690 nm) with an Infinite 200Pro Spectrophotometer (Tecan Group Ltd, Switzerland). Due to the large variations from experiment to experiment, TRAP activity values were normalized for each cell experiment to the mean of the 6 β-TCP batches in contact with osteoclasts.

2.5. Characterization of dissolution and osteoclastic resorption

A Field Emission Scanning Electron Microscope (FE-SEM, Merlin, Zeiss, Germany) was used to image β-TCP surfaces before and after the cell culture experiments.

Surface topography of the cylinders prior to and after the resorption experiments was measured with a non-contact 3-D profiler (S neox, Sensofar, Spain) using a 50x white light interferometry objective (50 × /0.55DI, CF plan, Nikon, Japan). Stitching was performed to enlarge the field of view up to 665 μm x 501 μm. For each repetition ($n = 6$) and each batch of β-TCP ($n = 6$), a total of 3 images per cylinders was acquired. Pseudo-colour images were generated with the software SensoMAP Premium (Version 7.4, Digital Surf, France) and the volume resorbed by the osteoclasts was extracted by determining the volume below a plane that was fitted to non-resorbed areas of the samples. To account for intrinsic differences of resorption between the 6 biological replicates, the mean resorbed thickness was normalized by the mean of the 6 β-TCP batches resorbed by osteoclasts.

After the 24 h cell culture experiments, the cell culture medium from each sample was recovered, centrifuged and the elemental concentrations of Ca, P, Na, K and Mg ions in the supernatant were quantified by ICP-MS. For this purpose, the cell culture medium was diluted directly (1:1000) in the acidic matrix solution. Then, the ^{44}Ca and ^{31}P isotopes were calibrated with the certified custom-made CaP standard solution, serially diluted to 5000:2500, 500:250, 100:50, 20:10 and 4:2 ppb. Other isotopes were calibrated with the 71A standard as already described for powders and cylinders. Finally, calibration drifts over time were corrected as already mentioned, with the internal standard and the repetitive measurements of the CaP and 71A standards. Concentrations were then normalized to Na, Mg and K mean values to account for volume fluctuations in the cell culture medium.

Table 2
Factors, levels, responses and sample sizes of β-TCP cylinders additionally used in the cell-culture experiments. The number of samples ($n = 6$) corresponds to the number of cylinders.

Factor	Levels	Responses		
		XPS	TRAP Activity	Mean resorbed thickness
Cell culture medium with no cells (NC), with macrophages (MA) and with osteoclasts (OC)	3	–	$n = 6$	$n = 6$
Ca/P molar ratio (bulk) of β-TCP cylinders (CaP1, CaP2, CaP3, CaP4, CaP5, CaP6)	6	$n = 6$	$n = 6$	$n = 6$

2.6. Statistical significance

Statistical analysis for all outcome measurements was conducted using Minitab software (Minitab, LLC, USA). Differences between treatment groups were assessed using factorial analysis model or one-way analysis of variance (ANOVA) with a post hoc, Bonferroni test. Linear correlation between variables was verified using a linear regression model. A *p*-value inferior to 0.01 was considered statistically significant.

3. Results

3.1. Synthesis of CDHA/β-TCP powders

The specific surface area (SSA) of CDHA and β-TCP powders can be visualized as a function of their bulk Ca/P molar ratio (XRD) in Fig. 1 and as a function of their calcination temperature and ICP-MS Ca/P molar ratio in Appendix A. The average SSA of CDHA powders was 108 ± 10 m^2/g ($n = 26$; Fig. 1a). A high variability was observed for Ca/P molar ratios close to 1.500: it varied from 120 m^2/g for a Ca/P molar ratio of 1.496 to 86 m^2/g for a Ca/P molar ratio of 1.502.

The mean SSA of β-TCP powders after calcination at 850 °C was 7 ± 2 m^2/g ($n = 26$; Fig. 1b) and was significantly lower ($p < 0.001$) than that of CDHA powders. There was a greater reproducibility between replicates of the triple measurements of CDHA powders (relative standard deviation of 0.8%; $n = 26$) than with those of β-TCP powders (relative standard deviation of 1.4%; $n = 26$). The Ca/P molar ratio had a significant effect on the SSA of β-TCP powders ($p < 0.001$). Specifically, the β-TCP powders showed significantly lower SSA of 5 ± 1 m^2/g ($p < 0.001$) at Ca/P molar ratios below 1.500 than at Ca/P molar ratios above 1.500 with 9 ± 1 m^2/g (Fig. 1b), with a significant change near the Ca/P molar ratio of 1.500 (Ca/P = 1.496; Fig. 1b). SEM images of these CDHA and β-TCP powders are presented in Appendix A.

3.2. Dense β-TCP cylinders characterizations

Representative surfaces of unpolished cylinders made from β-TCP powders calcined at 850 °C for 1 h are shown in Fig. 2. Qualitatively at Ca/P molar ratios inferior to 1.500 (Fig. 2a and b), grains were larger in size, and more easily recognizable. In addition, some porosity in cylinders with Ca/P molar ratios below 1.500 was seen (Fig. 2a and b),

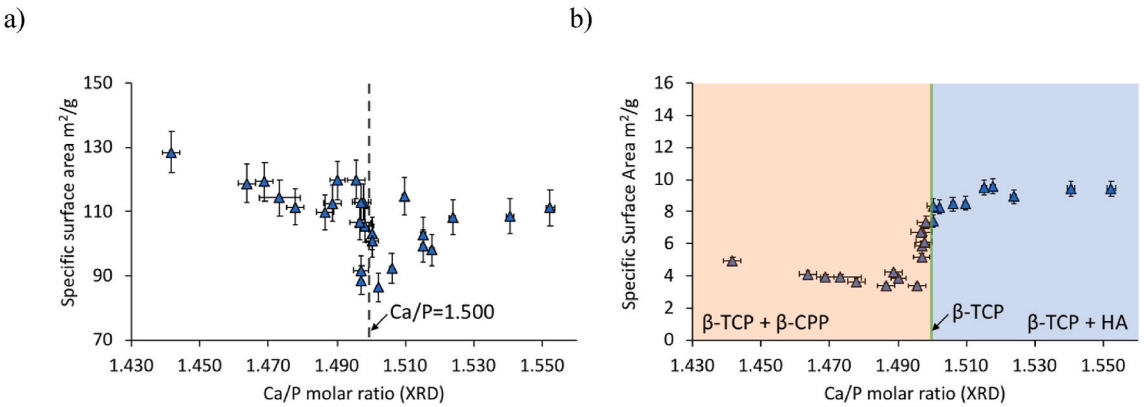

Fig. 1. Specific surface area (SSA) as a function of the Ca/P molar ratio measured by XRD. (a) SSA of CDHA powders obtained after synthesis; (b) SSA of β-TCP powders after thermal conversion (1 h at 850 °C). The colour code after calcination represents the phases quantified with the XRD analysis: orange for β-TCP + β-CPP, green for β-TCP and blue for β-TCP + HA. Vertical error bars stand for the uncertainty $U_{k=2}$ on SSA values and horizontal error bars represent the repeatability (2.77*estimated standard deviation of the Rietveld refinement).

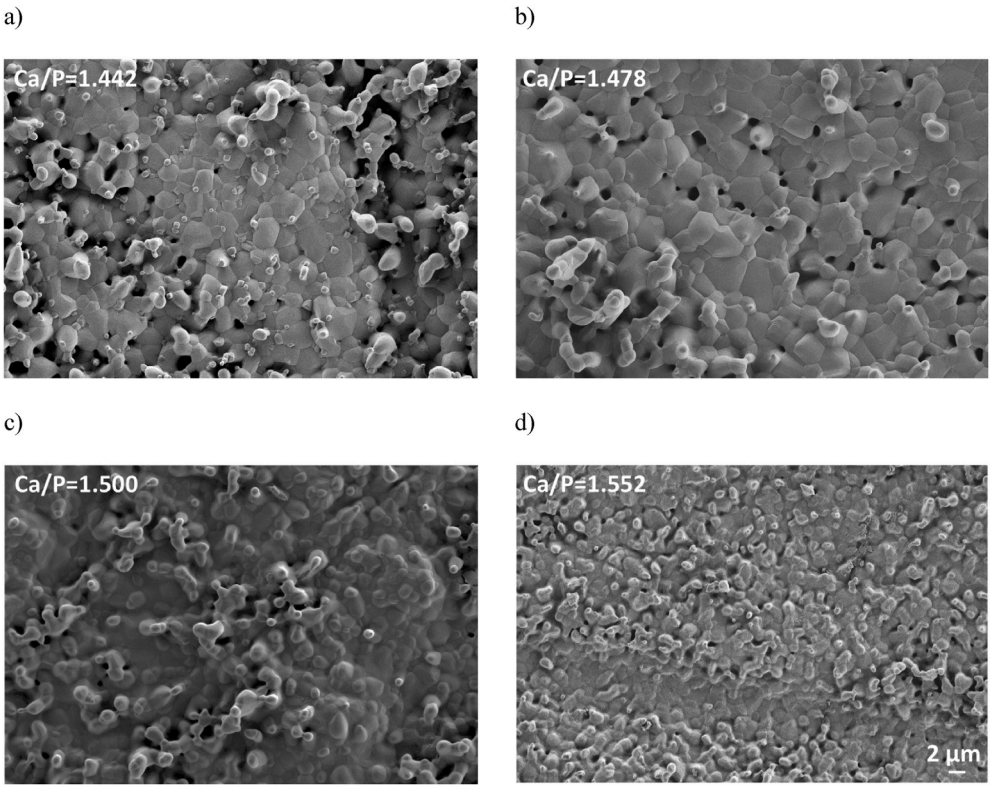

Fig. 2. SEM images of unpolished cylinders after 3 h of sintering at 1100 °C of 4 selected Ca/P molar ratios: (a) 1.442; (b) 1.478; (c) 1.500 and (d) 1.552. These cylinders were all made out of β-TCP powders calcined at 850 °C for 1 h. The scale bar is 2 µm for all 4 images.

whereas it was barely visible for cylinders with high Ca/P molar ratios (Fig. 2c and d). Quantitative results confirmed these findings (Fig. 3). Grain sizes of cylinders with a Ca/P molar ratio below 1.500 (mean: 2.11 ± 0.23 µm; Fig. 3a) were significantly larger ($p < 0.001$) than those of cylinders with Ca/P molar ratios greater than 1.500 (mean: 1.26 ± 0.26 µm; Fig. 3a).

Similarly, the Ca/P molar ratio (Fig. 3b) significantly affected cylinder densities ($p < 0.005$). The relative densities of cylinders with Ca/P molar ratios below 1.500 (Fig. 3b: mean relative density: 95.1 ± 1.8%) were significantly lower ($p < 0.001$) than those of cylinders with Ca/P molar ratios above 1.500 (Fig. 3b: mean relative density: 99.8 ± 0.3%).

The Ca/P molar ratio was not affected by the production of cylinders (Fig. 4). There was an excellent correlation (slope: 1.0001 and R^2 = 0.98) between the Ca/P molar ratio of the β-TCP powders and that of the cylinders. Details on the crystalline composition is shown in Appendix B.

Osteoclastic cell culture experiments were conducted with 6 batches of β-TCP cylinders varying in Ca/P molar ratio. The main bulk features of these batches are summarized in Table 3. Sr was the main contaminant (22 ppm) among the 43 elements considered by ICP-MS (Table 3 and Appendix B).

Surface chemistry of the β-TCP cylinders was analysed by XPS; the Ca/P, O/P and C/P ratios can be viewed in Fig. 5 as a function of their batch number (CaP1 to CaP6) or in other words according to their bulk (XRD) Ca/P molar ratio (1.496–1.502). The mean XPS Ca/P molar ratio was 1.39 ± 0.01, the mean O/P molar ratio was 4.92 ± 0.04 and the mean C/P molar ratio was 1.74 ± 0.13. Factorial analysis revealed that

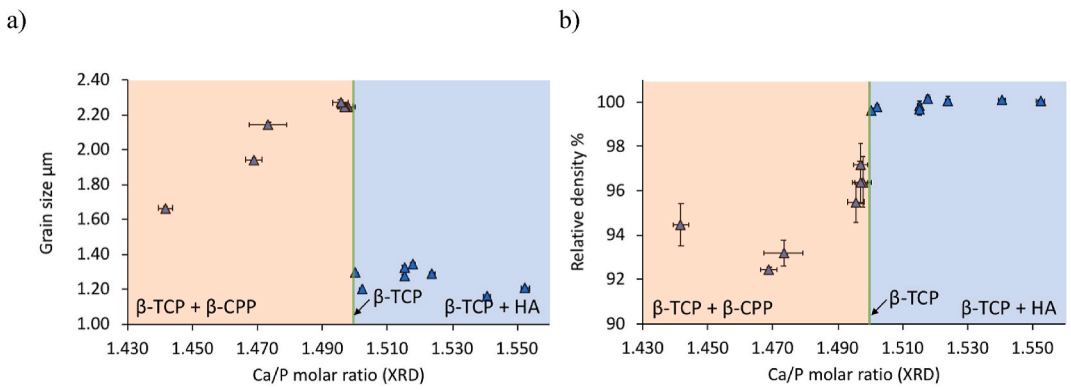

Fig. 3. Grain sizes (a) and relative densities (b) of β-TCP cylinders after sintering (3 h at 1100 °C) as a function of the Ca/P molar ratio measured by XRD. The colour code represents the phases quantified with the XRD analysis: orange for β-TCP + β-CPP, green for β-TCP and blue for β-TCP + HA. Error bars for the Ca/P molar ratio represent the repeatability (2.77*estimated standard deviation of the Rietveld refinement) while for the grain size it stands for the 99% confidence interval ($n = 3$; 3000 grains) and for the relative density for the standard deviation ($n = 3$).

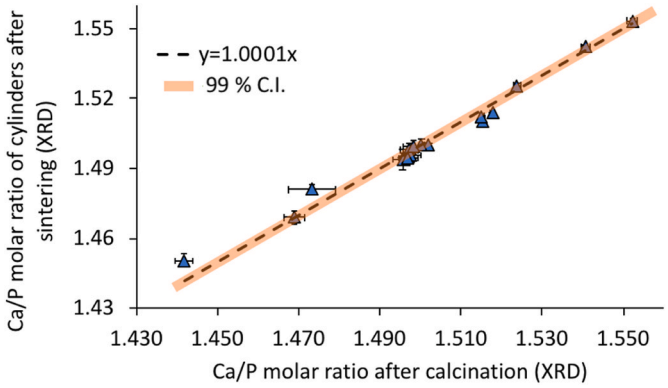

Fig. 4. Comparison of the Ca/P molar ratio measured by XRD after sintering of the cylinders (3 h at 1100 °C) and after the initial powder calcination (1 h at 850 °C). Black dashed curve represents the linear correlation between these two parameters (y = 1.0001x; $R^2 = 0.9784$) and orange highlighting stand for the 99% confidence interval (C·I.: 0.9983; 1.0019). Values are represented as mean ($n = 3$) ± their repeatability (2.77*estimated standard deviation of the Rietveld refinement).

Table 3
Main chemical characterization (XRD and ICP-MS) of β-TCP cylinders.

Batch	Bulk Ca/P molar ratio (XRD) –	Content of elemental impurities (ICP-MS)				
		Na ppm	Mg ppm	Sr ppm	Cu ppm	Fe ppm
CaP1	1.495 ± 0.002*	$<57^{LOD}$	$<6^{LOQ}$	19 ± 4**	$<1^{LOD}$	$<4^{LOD}$
CaP2	1.497 ± 0.002*	$<57^{LOD}$	$<6^{LOQ}$	20 ± 4**	$<1^{LOD}$	$<4^{LOD}$
CaP3	1.497 ± 0.002*	$<57^{LOD}$	$<6^{LOQ}$	19 ± 4**	$<1^{LOD}$	$<4^{LOD}$
CaP4	1.498 ± 0.002*	$<57^{LOD}$	$<6^{LOQ}$	20 ± 4**	$<1^{LOD}$	$<4^{LOD}$
CaP5	1.500 ± 0.001*	$<57^{LOD}$	$<6^{LOQ}$	21 ± 4**	$<1^{LOD}$	$<4^{LOD}$
CaP6	1.502 ± 0.001*	$<57^{LOD}$	$<6^{LOQ}$	20 ± 4**	$<1^{LOD}$	$<4^{LOD}$

*mean ± 2.77*ESD ($n = 3$); ** mean ± $U_{(k=2)}$ ($n = 3$); LOQ: Limit of quantification; LOD: Limit of detection.

there were no significant differences between the surface composition and the β-TCP batch number or the β-TCP bulk (XRD) Ca/P molar ratio.

3.3. TRAP staining and TRAP activities

TRAP staining confirmed that the multinucleated cells (number of nuclei >3) present in the cell culture medium were osteoclasts like cells (see pink-coloured cells, Fig. 6a, b, c and d). TRAP negative cells were also found. Comparison of the osteoclasts or multinucleated TRAP-positive cells present on the surface of β-TCP cylinders with low (Fig. 6a, c) and high (Fig. 6b, d) bulk (XRD) Ca/P molar ratios showed qualitatively no observable differences in terms of cell size, cell density and TRAP staining intensity. For comparison, one can see the development and spreading of osteoclasts along the 24 h experiment, in a tissue culture treated dish without cylinders (Appendix C). TRAP activity of the cells was quantified (Fig. 6e) for each type of β-TCP cylinder (CaP1 to CaP6; Ca/P = 1.496 to 1.502) and for each type of cell culture (cell culture medium with no cells NC, macrophages MA and osteoclasts OC). Factorial analysis showed that only the cell culture type had a significant effect ($p < 0.001$) on TRAP activity, while no significant effect of the bulk (XRD) Ca/P molar ratio was found. Significant levels of TRAP were quantified in cell cultures with osteoclasts only ($p < 0.001$), whereas no significant TRAP activity was quantified in cell culture medium with no cells and with macrophages, respectively.

3.4. SEM images of cell culture experiments

SEM images of β-TCP cylinders selected for some batches (CaP1: Ca/P = 1.496; CaP3: Ca/P = 1.497; CaP5: Ca/P = 1.500 and CaP6: Ca/P = 1.502) can be viewed in Fig. 7 prior to the cell culture experiment ("initial state"; first column), and after 24 h of cell culture experiments with cell culture medium with no HCl and no cells (Fig. 7; second column), with cell culture medium with HCl and with no cells (Fig. 7; third column), with macrophages (Fig. 7; fourth column) and finally with osteoclasts (Fig. 7; fifth column). Additional SEM images of β-TCP cylinders with very high Ca/P molar ratio (1.516) can be consulted in Appendix D. After polishing, it was possible to observe the decrease in porosity from batch CaP1 (Ca/P = 1.496) to batch CaP6 (Ca/P = 1.502). On all these polished surfaces, it was difficult to easily distinguish the grains. After 24 h of contact with the cell culture medium (without cells and HCl), the surfaces were slightly dissolved, especially along the polishing lines and the grain boundaries. This dissolution appeared slightly more pronounced in the presence of HCl and macrophages. A marked difference was seen in the presence of osteoclasts: some areas on the surface of the cylinders (in contact with osteoclasts) were resorbed while some others were not. Overall, the SEM images (Fig. 7) revealed

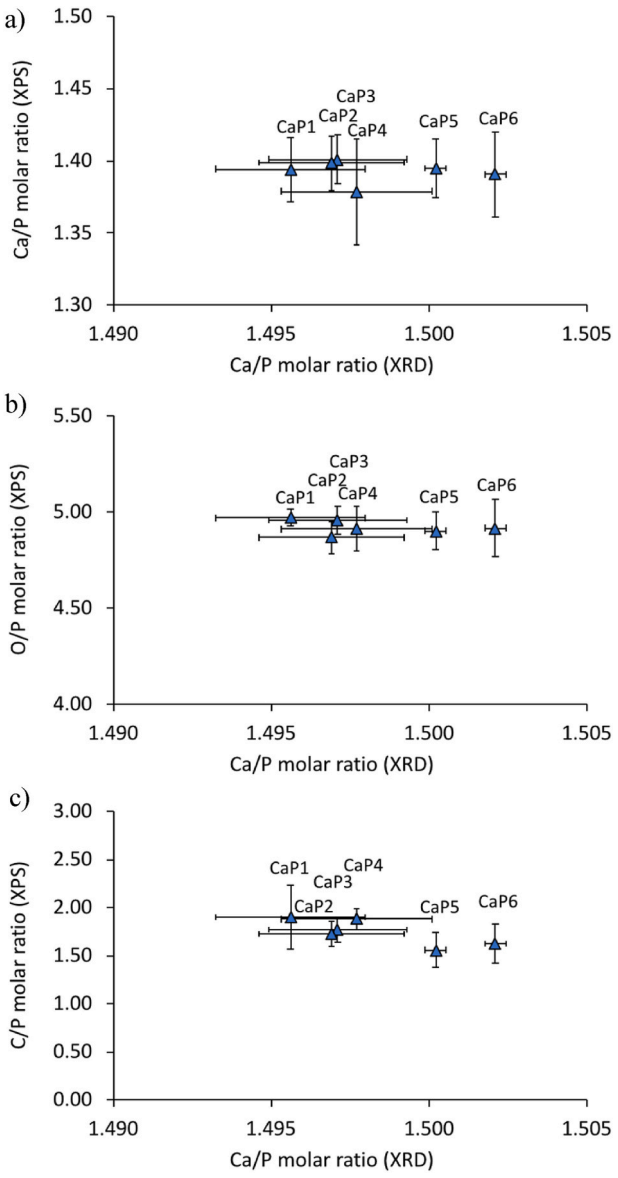

Fig. 5. XPS analysis of selected batches of β-TCP cylinders (CaP1: Ca/P = 1.496, CaP2: Ca/P = 1.497, CaP3: Ca/P = 1.497, CaP4: Ca/P = 1.498, CaP5: Ca/P = 1.500 and CaP6: Ca/P = 1.502) prior to the cell culture experiments; (a) Ca/P molar ratio; (b) O/P molar ratio and (c) C/P molar ratio. Vertical error bars stand for standard deviations (n = 3) and horizontal error bars for reproducibility (2.77*estimated standard deviation).

that the resorption of β-TCP cylinders was inhomogeneous, regardless of their Ca/P molar ratio. The resorbed grains presented highly oriented pits/needles on their surfaces.

White-light interferometry (WLI) was used to analyse the topography of polished β-TCP cylinders. Green colour on these pseudo-colour images represents the reference plane while blueish colour gradients represent areas below this plane, namely areas resorbed by the osteoclasts. The topography of β-TCP cylinders in contact with the cell culture medium with no cells (Fig. 8a) or with macrophages (Fig. 8b) was rather flat, with a predominance of the green colour. In addition, some scratches from polishing were indicated by black arrows in Fig. 8a and b. Conversely, the topography of β-TCP cylinders in contact with osteoclasts (Fig. 8c, d, e and f) exhibited valleys from resorbed areas (blueish colour gradients) and non-resorbed areas (green colour). The valleys showed the resorption path of osteoclasts, indicated by white arrows.

Further analysis of these topographies (Fig. 9), allowed to quantify the mean thickness resorbed by the cells as a function of the Ca/P molar ratio and the type of cell culture (NC, MA and OC). Factorial analysis of these results revealed that the cell culture type (Fig. 9a) and the bulk Ca/P molar ratio (Fig. 9b) had a significant effect ($p < 0.001$) on the mean resorbed thickness; while the repetition of the cell experiments was found non-significant. The mean resorbed thickness was significantly higher for β-TCP cylinders in contact with the osteoclasts ($p < 0.001$) than for cylinders in contact with no cells (NC) or with macrophages (MA); no significant difference between the latter two groups was found. Comparison of the resorption between the different β-TCP batches showed that the batch CaP5 (Ca/P = 1.500) was significantly more resorbed ($p < 0.001$) compared to batches CaP1 (Ca/P = 1.496), CaP2 (Ca/P = 1.497) and CaP6 (Ca/P = 1.502). Interestingly, for Ca/P molar ratios below 1.500, there was a linear positive correlation (y = 6.086x – 9.054; r = 0.967; $p = 0.007$) between the mean resorbed thickness and the Ca/P molar ratio.

3.5. ICP-MS analysis of cell culture medium

According to the ICP-MS measurements, only the Ca and P ion concentrations were significantly affected by the cell culture type ($p < 0.001$; Fig. 10a and b), whereas the Ca/P molar ratios and the concentrations of Na, K, Mg ions in the cell culture medium were not influenced by any of the studied factors (Fig. 10c, d, e and f). Further comparisons between the cell culture types showed that Ca and P ion concentrations in the cell culture medium of β-TCP cylinders in contact with osteoclasts (OC) were significantly higher than their basal values ($p \leq 0.001$; Fig. 10a and b): 2.05 ± 0.19 mM ($n = 6$) and 1.29 ± 0.13 mM ($n = 6$), respectively. Conversely, no significant difference in Ca and P ion concentrations was found between the cell culture medium of β-TCP cylinders in contact with no cells (NC) or macrophages (MA) and their basal concentrations (Fig. 10a and b). Also, in the presence of osteoclasts, no significant differences in the Ca and P ion concentrations were found in between all the different batches (CaP1 to CaP6).

3.6. Comparison of β-TCP resorption with WLI and ICP-MS

β-TCP resorbed masses were estimated from WLI and ICP-MS measurements according to eq. (1) and eq. (2), respectively. The calculated masses were compared in Fig. 11. Statistical analysis, showed that there was a non-significant ($p = 0.338$) negative correlation between these two variables (r = −0.478; $R^2 = 0.228$).

$$m_{resorbed_{WLI}} = \mu_{resorbed} \cdot \pi \cdot \left(\frac{d}{2}\right)^2 \cdot \rho_{\beta-TCP} \quad \text{(eq.1)}$$

Where $\mu_{resorbed}$ is the mean resorbed thickness, d the mean cylinder diameter (d = 5.48 ± 0.03 mm ($n = 4$) [35]) and $\rho_{\beta-TCP}$ the theoretical density of β-TCP (3070 kg/m^3 [40]).

$$m_{resorbed_{ICP-MS}} = \frac{1}{2} \cdot ([P]_{OC} - [P]_{NC\ and\ MA}) \cdot V_{tot} \cdot M_{\beta-TCP} \quad \text{(eq.2)}$$

Where the $[P]_{OC} - [P]_{NC\ and\ MA}$ is the P ion concentration released in the cell culture medium, V_{tot} the volume of liquid in each well (150 μL), $M_{\beta-TCP}$ the molecular weight of β-TCP (310.177 g/mol) and the factor (1/2) to account that there are 2 mol of P in 1 mol of β-TCP ($Ca_3(PO_4)_2$).

4. Discussion

This study investigated the effect of the Ca/P molar ratio on the physico-chemical and the osteoclastic resorption of β-TCP cylinders. Since grain size, porosity, topography and surface chemistry could affect the results, an attempt was made to keep these latter parameters constant while varying the Ca/P molar ratio. However, this could not be achieved, since the Ca/P molar ratio affected some of these parameters. Importantly, ISO 17025 accredited XRD and ICP-MS methods were used

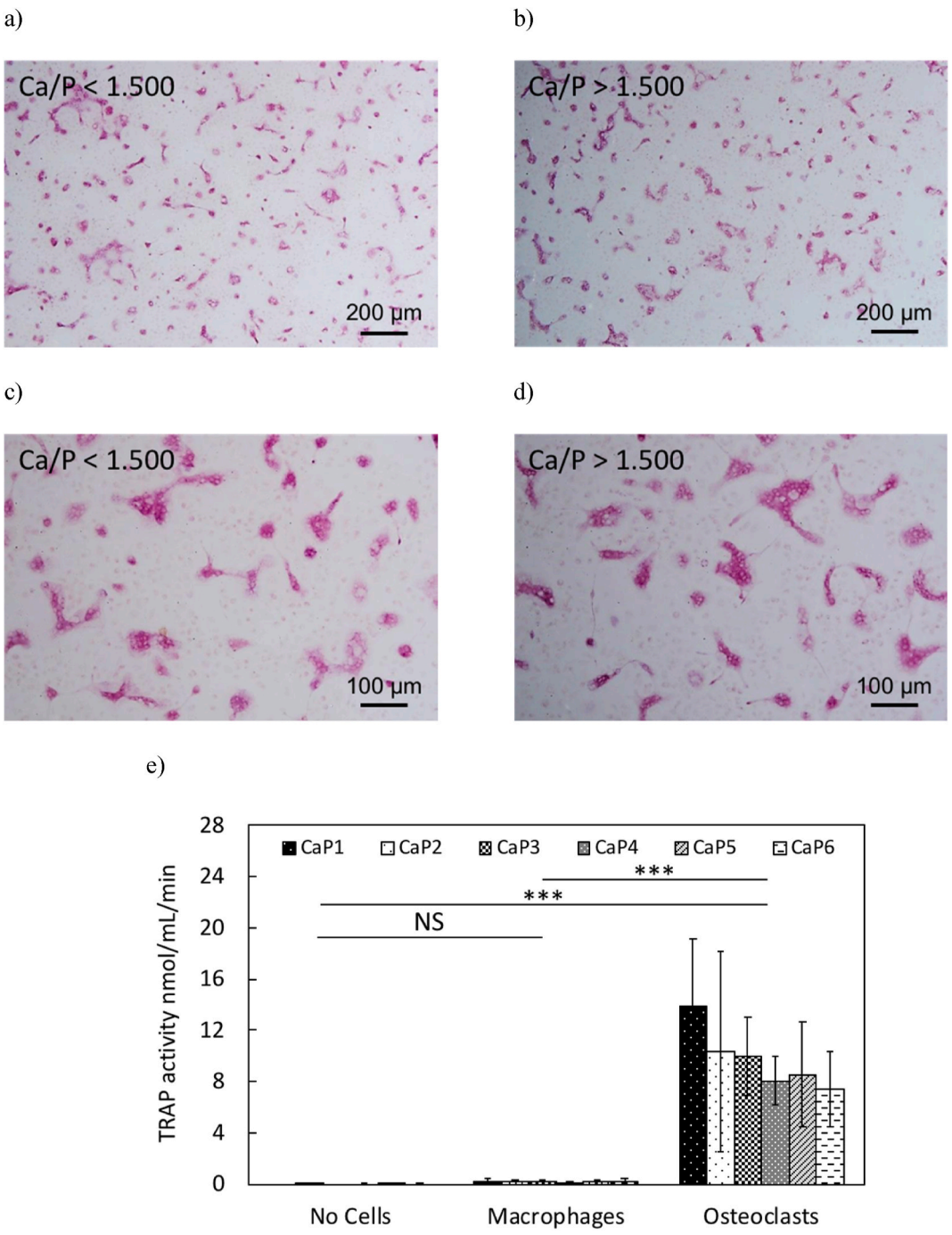

Fig. 6. Optical microscope images of TRAP stained osteoclasts on polished β-TCP cylinders with a Ca/P molar ratio lower than 1.500 (a and c) and greater than 1.500 (b and d). Scale bars represent either 100 or 200 µm. (e) TRAP Activity of cells after 24 h of cell culture experiment on all polished β-TCP cylinders from all batches (CaP1: Ca/P = 1.496, CaP2: Ca/P = 1.497, CaP3: Ca/P = 1.497, CaP4: Ca/P = 1.498, CaP5: Ca/P = 1.500 and CaP6: Ca/P = 1.502) with cell culture medium with no cells (NC), macrophages (MA) and osteoclasts (OC). Data were normalized by the mean of each cell experiment. Error bars stand for standard deviations ($n = 5$). Relative comparisons with the Bonferroni correction are indicated by: ***($p < 0.001$) and NS (non-significant).

to determine the Ca/P molar ratios of powders/cylinders. XRF was not used since it does not provide more accurate results than XRD and ICP-MS in the considered Ca/P molar ratio range.

4.1. Specific surface area of CDHA powders

The SSA values of the synthesized CDHA powders were high and ranged between 80 and 130 m^2/g depending on the Ca/P molar ratio (Fig. 1a). In particular, the change in particle geometry could explain the evolution of the SSA of CDHA powders with the Ca/P molar ratio; it also justifies why the apparent volume of 1 g of CDHA powder with low Ca/P molar ratio was larger compared to 1 g of CDHA powder with high Ca/P molar ratio (Appendix A). Despite these variations, the SSA values were consistent with those reported in the literature by Descamps et al. (superior to 60 m^2/g) [26] or by Destainville et al. (89 ± 2 m^2/g) [32]. SEM imaging of CDHA powders (Appendix A) showed agglomerated particles in the nanometric range, as also observed by Destainville et al. [32]. These variations of the specific surface area were mainly explained by the change in pH during the synthesis, as previously shown by Blumenthal et al. [41], Raynaud et al. [42,43] and Le Gars Santoni et al. [34].

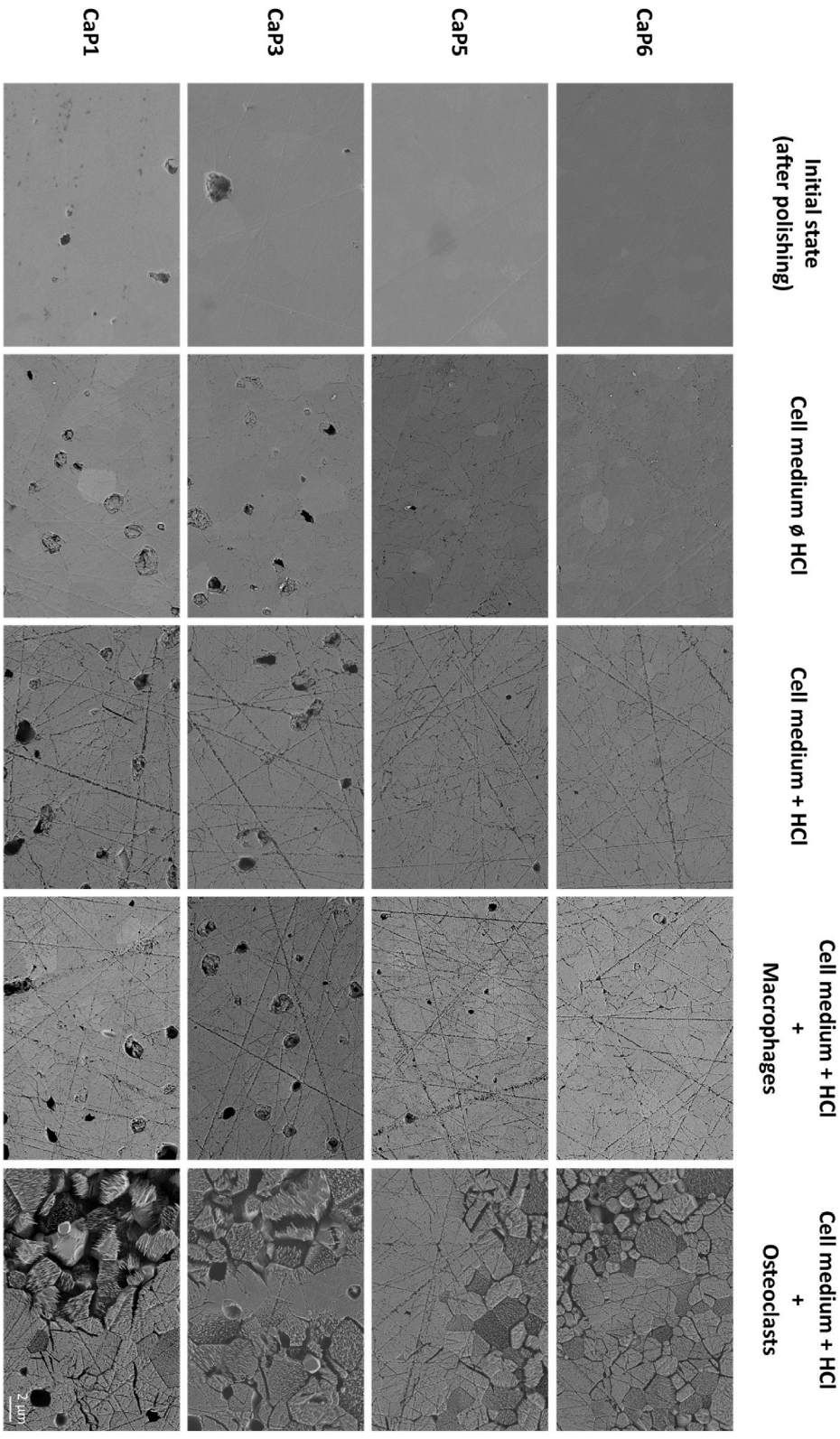

Fig. 7. Representative SEM images of the surface of β-TCP cylinders from batch CaP1 (Ca/P = 1.496); CaP3 (Ca/P = 1.497); CaP5 (Ca/P = 1.500) and CaP6 (Ca/P = 1.502), before cell culture, after 24 h in cell culture medium without and with HCl, with macrophages and with osteoclasts. The scale bar is the same for all images and represents 2 μm.

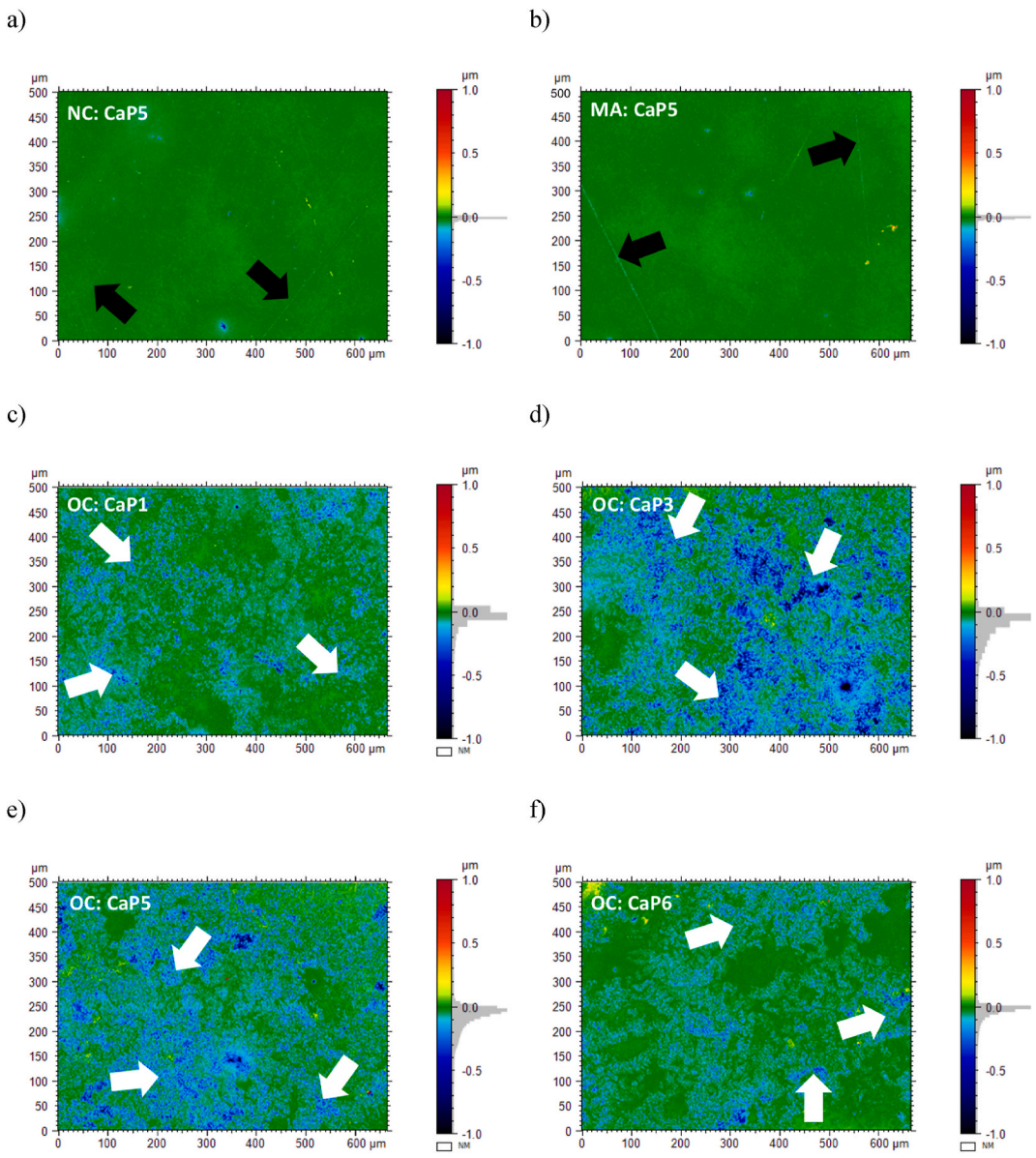

Fig. 8. Representative pseudo-colour images of the surface of polished β-TCP cylinders from white light interferometry measurements. Image (a) shows batch CaP5, with a Ca/P of 1.500 after 24 h of contact with cell culture medium with no cells (NC) and image (b) after 24 h with macrophages (MA); images (c), (d), (e) and (f) represent batches CaP1 (Ca/P = 1.496), CaP3 (Ca/P = 1.497), CaP5 (Ca/P = 1.500) and CaP6 (Ca/P = 1.502) after 24 h of contact with osteoclasts (OC). Green colour represents the reference plane and blueish colours the zones below this reference. In the case of images (c), (d), (e) and (f), blueish colours show the areas resorbed by the osteoclasts (white arrows). Black arrows indicate lines from mechanical polishing.

4.2. Specific surface area of β-TCP powders

The SSA of β-TCP powders varied drastically at a Ca/P molar ratio of 1.500 (Fig. 1b), as also noted by Descamps et al. [26]. This abrupt change was confirmed by SEM images which showed a significant reduction in particle size for Ca/P molar ratios above 1.500 (Appendix A); however, the SSA values reported by Descamps et al. were much lower because their powders were calcined at higher temperature (950 °C) [26]. Similar trends of the SSA of calcined calcium phosphate powders was also shown by Raynaud et al. [43].

4.3. Sinterability of β-TCP cylinders

Near full density samples were obtained with Ca/P molar ratios greater than 1.500 (Fig. 2). Importantly, the fabrication process did not alter the bulk Ca/P molar ratio between initial powders and final cylinders (Table 3, Fig. 4 and Appendix B). Their grain sizes were significantly reduced (Fig. 3a) and their relative densities were significantly increased (Fig. 3b) compared to samples with a Ca/P molar ratio inferior to 1.500. Similar observations were made by Descamps et al. [44]. These authors obtained cylinders with high relative densities (>99.6%) and with a significant reduction of the grain sizes (1.83–1.51 µm) between Ca/P molar ratios of 1.500 and 1.548.

Conversely, cylinders with Ca/P molar ratios inferior to 1.500 were less well sintered than cylinders with higher Ca/P molar ratios (Fig. 2): grain sizes were larger (2.11 ± 0.23 µm; Fig. 3a) and relative densities were lower (95.1 ± 1.8%; Fig. 3b). This suggests different grain growth rates as a function of the Ca/P molar ratio. This phenomenon of abnormal grain growth has also been reported by Descamps et al. [26] and by Raynaud et al. [43] or Champion [45] who noticed a reduction in sinterability for β-TCP cylinders with Ca/P molar ratios below 1.500.

The comparison of the sinterability of the cylinders as a function of

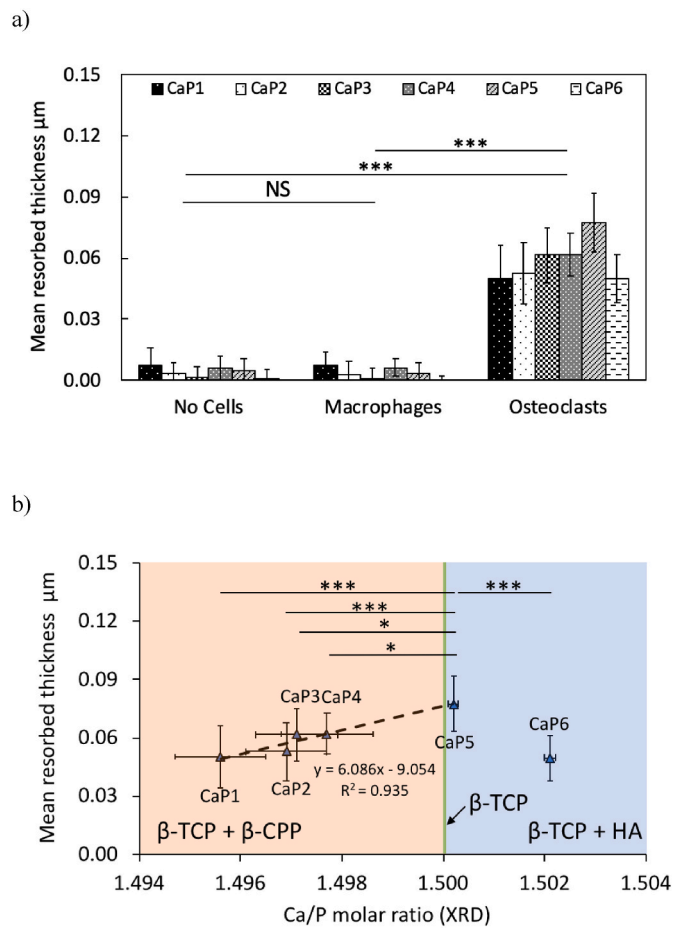

Fig. 9. (a) Mean resorbed thickness after 24 h of cell experiments with cell culture medium with no cells (NC), with macrophages (MA) and with osteoclasts (OC) on all β-TCP cylinders from all batches (CaP1: Ca/P = 1.496, CaP2: Ca/P = 1.497, CaP3: Ca/P = 1.497, CaP4: Ca/P = 1.498, CaP5: Ca/P = 1.500 and CaP6: Ca/P = 1.502). The mean surface roughness (Ra) of the cylinders before immersion is 4.5 ± 1.3 nm. (b) Mean resorbed thickness of all batches of β-TCP cylinders (CaP1 to CaP6) in contact with osteoclasts as a function of their Ca/P molar ratio. The dashed line represents the linear positive correlation (Pearson's coefficient r = 0.967; R^2 = 0.935; p = 0.007; y = 6.086x – 9.054) between the mean resorbed thickness and Ca/P molar ratios ≤ 1.500. The colour code represents the phases quantified by the XRD analysis: orange for β-TCP + β-CPP, green for β-TCP and blue for β-TCP + HA. To allow for comparisons, data were normalized to the mean osteoclastic values from each repetition of the cell experiment. Error bars stand for standard deviations: n = 6. Relative comparisons with the Bonferroni correction are indicated by: ***(p < 0.001), *(p < 0.05) and NS (non-significant).

the initial powder calcination temperature (775 °C or 850 °C; Appendix E) showed that despite the modification of the SSA (Appendix A), the sinterability of the cylinders (grain sizes and densities) was not significantly influenced. This means that the modification of the sinterability was mostly related to the bulk Ca/P molar ratio of the powders and potentially to the presence of secondary phases i.e. HA or β-CPP.

4.4. Surface chemistry and roughness of β-TCP cylinders

Surface chemistry and topography are known to affect the biological response [30,31]. For this reason, the samples were polished and the surface topography and chemistry of the polished surface were measured. There was no significant difference between the surface roughness of all β-TCP cylinders, whose mean roughness (Ra) was 4 ± 1 nm (Appendix F). XPS analysis did not reveal any significant difference of surface composition between the different batches of β-TCP cylinders (Fig. 5). However, the XPS Ca/P molar ratios were all lower compared to the bulk values, as reported in many studies [46–48]. Chusuei et al. [47] and Lu et al. [46] attributed these lower values to material decomposition due to prolonged exposure to X-rays. However, this explanation was refuted by Kleine-Boymann et al. [48] who demonstrated that a 30-min exposure of a calcium phosphate pellet to X-rays did not alter the surface concentration of Ca, P and O. This group also checked whether a P-enriched surface was possible on bulk samples with low Ca/P molar ratios and found no significant changes in the XPS Ca/P molar ratio with increasing sample depth [48]. One explanation for these lower Ca/P molar ratio is that the PO_4 groups may be more dominant on the surface, due to an orientation effect, with PO_4 groups on the outside and Ca ions in the centre.

This surface analysis also revealed that the O/P and C/P molar ratios were slightly higher than the overall theoretical values (4 and 0, respectively). This was due to a slight organic contamination on the surface of the cylinders, possibly due to the polishing and cleaning procedure.

4.5. Osteoclasts cell culture

Cell adhesion was optimized on β-TCP cylinders with a protein layer made with the FBS coating prior to the resorption experiments [49]. The formation of osteoclasts from hematopoietic stem cells requires the presence of M-CSF and RANKL in the cell culture medium [50,51]. To dissociate the resorption effect from osteoclasts, a cell culture group containing monocytes/macrophages was included in this study: the macrophage group (MA). In addition, HCl was added to the cell culture medium to activate the resorption capacity of osteoclasts [52], hence the group "cell culture medium with no cells" (NC) was also investigated in order to dissociate the possible dissolution of calcium phosphate due to the acidity of the cell culture medium for the osteoclastic resorption.

TRAP staining and TRAP activity (Fig. 6) agreed on the presence of multinucleated TRAP positive cells or osteoclasts (number of nuclei greater than 3) on the surface of the β-TCP cylinders of the cell culture group "osteoclasts" (OC). Interestingly, the substrate was shown to significantly affect the morphology of osteoclasts. Osteoclasts grown on TCT plates appeared larger in size, with many nuclei and with a round shape (Appendix C), in contrast osteoclasts seeded on β-TCP cylinders had a smaller size with an irregular shape and fewer nuclei (Fig. 6). These differences in osteoclasts morphology were also reported in the literature [53]. The cylinders had no significant effect of the TRAP activity of the osteoclasts. Since the TRAP activity is a measure that depends on the number of osteoclasts [54], on their resorptive activity [54,55], and on surface roughness [56,57], an absence of TRAP activity change may indicate that all parameters were constant or that some parameters had an influence in opposite directions.

4.6. Resorption experiments

The slight dissolution of the β-TCP cylinders placed in the cell culture medium (Fig. 7) was unexpected since β-TCP is insoluble in these conditions [21]. Grain boundaries dissolution could be due to a different chemical composition/solubility than β-TCP. In fact, a recent study by Maazouz et al. [58] pointed out that a layer consisting of a "basic calcium-rich phase" could cover the surface of β-TCP particles, possibly $Ca(OH)_2$ or $CaCO_3$, as shown by Döbelin et al. [59]. In addition, grain boundaries have lower densities and contain defects which can facilitate their dissolution. Surface dissolution, in particular along the polishing lines, could be due to the presence of small amounts of an amorphous phase created during polishing. For example, Gbureck et al. [60] showed that such an amorphous phase appeared during β-TCP milling and led to a much more reactive powder.

The surfaces of the β-TCP cylinders in contact with osteoclasts had a distinct morphology (Fig. 7). The resorbed grains had highly oriented pits/needles on their surfaces. These characteristics are explained by the

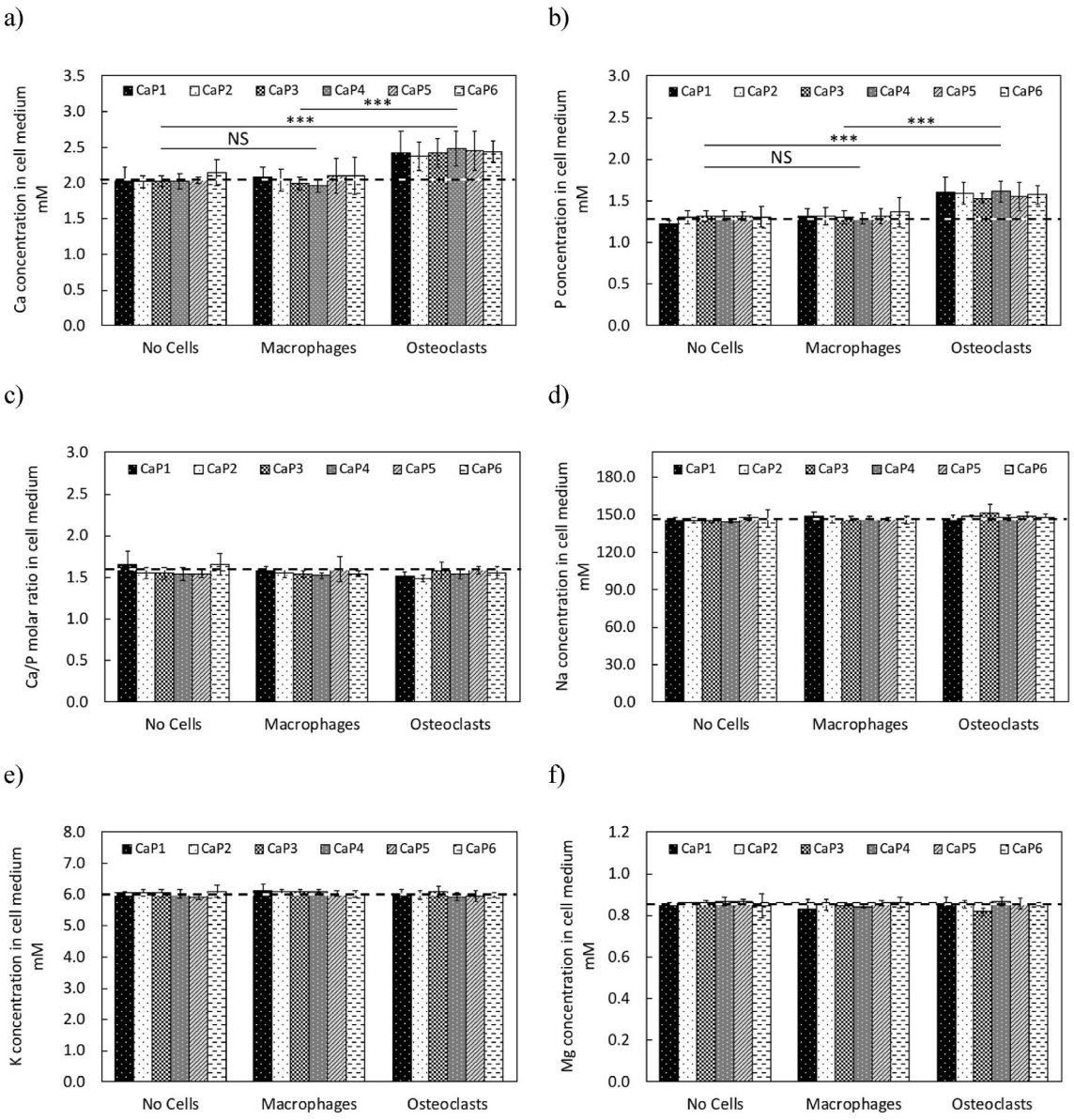

Fig. 10. ICP-MS analysis of the cell culture medium after 24 h of cell experiment on all β-TCP cylinders (CaP1: Ca/P = 1.496, CaP2: Ca/P = 1.497, CaP3: Ca/P = 1.497, CaP4: Ca/P = 1.498, CaP5: Ca/P = 1.500 and CaP6: Ca/P = 1.502) in contact with cell culture medium with no cells (NC), with macrophages (MA) and with osteoclasts (OC); (a) Ca ion concentration; (b) P ion concentration; (c) Ca/P molar ratio; (d) Na ion concentration; (e) K ion concentration and (f) Mg ion concentration. The dashed horizontal lines represent the corresponding basal ion concentration in the cell culture medium: 2.05 ± 0.19 mM for Ca, 1.29 ± 0.13 mM for P, 1.59 ± 0.07 for Ca/P molar ratio, 146.88 ± 0.94 mM for Na, 6.01 ± 0.13 mM for K and 0.86 ± 0.02 mM for Mg. Error bars stand for standard deviations ($n = 6$). Relative comparisons with the Bonferroni correction are indicated by: ***($p < 0.001$) and NS (non-significant).

fact that osteoclasts are able to secrete locally an acidic environment with pH values of 3.9–4.5 under their body [12], thus making β-TCP dissolution possible. Several studies have also reported a similar topography of grains resorbed by osteoclasts [12,61]. Recently, Gallo et al. demonstrated that the orientation of these pits/needles on the surface of the grains corresponded to the *c*-axis of the β-TCP crystal, making the resorption a crystallographically mediated process [35]. In addition, it was possible to distinguish the presence of non-resorbed crystals in β-TCP cylinders with Ca/P molar ratio superior to 1.500 (Appendix E), likely hydroxyapatite since this latter is roughly one order of magnitude less soluble than β-TCP [29].

Since osteoclastic resorption was inhomogeneous, no conclusions could be drawn with the SEM images (Fig. 7) nor with the pseudo-colour images (Fig. 8) alone. For this reason, osteoclastic resorption was quantified with a topographically sensitive technique (Fig. 9). One possibility would have been to quantify the resorption with SEM-FIB, but this is a laborious technique requiring numerous FIB preparation/manipulation steps [62]. A non-contact 3-D profilometry technique, based on white light interferometry was preferred [63] since quantification was directly done with the microscope software; however, this method required polished samples for appropriate measurements. In particular, the resorption was quantified by the parameter "mean resorbed thickness", because the mean resorbed area could be biased by the selection of the zone on the cylinders that could be more or less resorbed [54].

ICP-MS was used as a second method to quantify the osteoclastic resorption, via the increase of the Ca and P ion concentrations in the cell culture medium (Fig. 10). The values of osteoclastic resorption, quantified by WLI and ICP-MS were relatively close (Fig. 11). However, based on the calculation hypothesis, the resorption quantified by ICP-MS

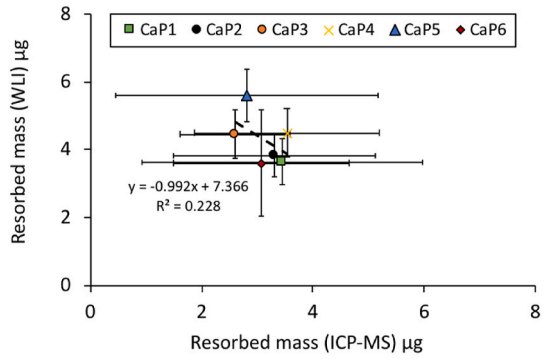

Fig. 11. Comparison of masses of β-TCP resorbed by osteoclasts on the upper surface of CaP1 to CaP6 cylinders, quantified by white light interferometry (y axis) and by ICP-MS (x axis) via phosphate release in the cell culture medium. The Pearson's correlation coefficient r was −0.478, R^2 value was 0.228 and *P* value was 0.338. Error bars stand for standard deviations ($n = 6$).

should have been higher than that quantified by WLI. In addition, there was an absence of correlation between these two methods. All these differences may be due to the high standard deviations on the ICP-MS results or to a slight precipitation of apatite in the cell culture medium. This also explains why with ICP-MS no significant differences were seen in the ion concentrations of the resorbed cylinders.

The bulk Ca/P molar ratio had a significant effect on the osteoclastic resorption of β-TCP cylinders (Fig. 9): it was maximum for a Ca/P molar ratio close to 1.500 (CaP5). These modulations of osteoclastic resorption may be the consequences of chemical (secondary phases) and physical (grain size, density, surface area) modifications induced by the Ca/P molar ratio on the cylinders. At Ca/P molar ratios below 1.500 (batches CaP1 to CaP4), there was no significant change of grain size; so, this latter cannot be invoked to explain the change in osteoclastic resorption. The decrease in grain size observed for Ca/P molar ratio above 1.500 (Fig. 3a) may lead to an increased resorption [64,65]. However, the osteoclastic resorption decreased (Fig. 9), indicating that the change in grain size did not influence the osteoclastic resorption. Conversely, by increasing the Ca/P molar ratio, the density of the cylinders increased by 5%. This increase of density decreased the total surface area, which should decrease the osteoclastic resorption [65,66]. But, between the CaP5 and CaP6 batches, the density of the cylinders did not change; hence it cannot explain the decrease in osteoclastic resorption observed.

Recently, it was found that at least two β-TCP structures with different lattice parameters co-exist [34]: "β-TCP(−)" is dominant at a Ca/P molar ratio below 1.500 while "β-TCP(+)" is dominant at a Ca/P molar ratio above 1.500. However, there is currently no information on the relative solubility and the osteoclastic resorption of these structures. Since differences in resorption were noted with the Ca/P molar ratio, it is possible that these two structures are also more or less prone to osteoclastic resorption.

The composition or the presence of secondary phases may have played a role: pyrophosphates [67,68] are known to reduce osteoclastic resorption and HA is difficult to resorb [25,29]. Indeed, a significant decrease in resorption was observed by decreasing the Ca/P molar ratio to 1.496 (CaP1), which is associated with an increase in β-CPP (<1 wt %). Similarly, by increasing the amount of HA between the CaP5 and CaP6 batches (0.2 and 1.3 wt% respectively), there was a decrease in resorption. Thus, β-TCP resorption was the highest in the absence of the secondary phases (β-CPP and HA). The 40% decrease in resorption with a β-CPP content below 1 wt% is remarkable considering that β-TCP can contain up to 5 wt% β-CPP and still be sold as "β-TCP".

5. Conclusion

To summarize, this study showed that the bulk Ca/P molar ratio influenced the physico-chemical properties of β-TCP powders/cylinders and their osteoclastic resorption. In particular, the increase in the bulk Ca/P molar ratio increased the SSA of the β-TCP cylinders with a consequent increase near a Ca/P molar ratio of 1.500. Similarly, the increase in the Ca/P molar ratio increased the density of the cylinders and significantly reduced the grain size, with a drastic change near a Ca/P molar ratio of 1.500. Importantly, the slip casting and sintering process did not change the initial phase purity and the content of elemental impurities in the cylinders; these cylinders were among the purest in terms of elemental impurities reported in the literature [34]. In terms of surface chemistry, the bulk Ca/P molar ratio did not change the Ca/P molar ratio on the surface and the TRAP activity of the osteoclasts. SEM imaging showed no precipitation of any calcium phosphate phase on the surface of the β-TCP cylinders in the cell culture medium without and with cells. Additionally, it highlighted the osteoclastic resorption, as the surface of resorbed β-TCP cylinders had a distinct morphology compared to the surface of cylinders in contact with the cell culture medium with no cells or with macrophages. ICP-MS analysis of the cell culture medium confirmed the osteoclastic resorption, with a significant release of Ca and P ions with a Ca/P molar ratio close to 1.500. White light interferometry was a potent and sensitive method to quantify the osteoclastic resorption. The linear effect of β-CPP on β-TCP resorption is remarkable since the presence of 1% β-CPP reduced β-TCP resorption rate by 40%. β-CPP effect is attributed to the inhibitory action of pyrophosphate ions on osteoclasts. Even though these results are in vitro, they suggest that the assessment of β-TCP biological properties should always include a discussion on the β-CPP content. This study also suggests that the β-CPP content can be used to modulate the osteoclastic resorption of β-TCP bone graft substitutes and to some extend control bone repair; however, this must be confirmed by an in vivo study.

CRediT authorship contribution statement

B. Le Gars Santoni: Conceptualization, Methodology, Validation, Formal analysis, Investigation, Writing – original draft, Visualization. **L. Niggli:** Investigation. **S. Dolder:** Investigation. **O. Loeffel:** Investigation. **G.A. Sblendorio:** Investigation. **R. Heuberger:** Methodology, Writing – review & editing. **Y. Maazouz:** Formal analysis. **C. Stähli:** Methodology, Validation, Writing – review & editing. **N. Döbelin:** Methodology, Software, Validation. **P. Bowen:** Conceptualization, Writing – review & editing, Funding acquisition. **W. Hofstetter:** Conceptualization, Resources, Writing – review & editing. **M. Bohner:** Conceptualization, Formal analysis, Resources, Writing – review & editing, Supervision, Project administration, Funding acquisition.

Declaration of competing interest

None.

Acknowledgements

The authors acknowledge Pascal Michel and Isabelle Heimgartner for their technical support, Jean-Christophe Hornez for his advice with the slip casting procedure and the Swiss National Science Foundation for its funding (Grant no. 200021_169027).

Appendix A. Supplementary data

Supplementary data to this article can be found online at https://doi.org/10.1016/j.bioactmat.2021.09.003.

References

[1] M. Bohner, L. Galea, N. Doebelin, Calcium phosphate bone graft substitutes: failures and hopes, J. Eur. Ceram. Soc. 32 (2012) 2663–2671, https://doi.org/10.1016/j.jeurceramsoc.2012.02.028.

[2] P.V. Giannoudis, H. Dinopoulos, E. Tsiridis, Bone substitutes: an update, Injury 36 (2005) 20–27, https://doi.org/10.1016/j.injury.2005.07.029.

[3] Frost Sullivan, European Markets for Bone Grafts and Bone, 2008.

[4] J. j Park, S. h Hershman, Y. h Kim, Updates in the Use of Bone Grafts in the Lumbar Spine, in: Bulletin of the Hospital for Joint Diseases, vol. 71, J. Michael Ryan Publishing Inc, 2013, pp. 39–48.

[5] T.A. St John, A.R. Vaccaro, A.P. Sah, M. Schaefer, S.C. Berta, T. Albert, A. Hilibrand, Physical and monetary costs associated with autogenous bone graft harvesting, Am. J. Orthoped. 32 (2003) 18–23.

[6] A. Van Heest, M. Swiontkowski, Bone-graft substitutes, Lancet 353 (1999) S28–S29, https://doi.org/10.1016/S0140-6736(99)90228-3.

[7] J.C. Banwart, M.A. Asher, R.S. Hassanein, Iliac crest bone graft harvest donor site morbidity. A statistical evaluation, Spine 20 (1995) 1055–1060, https://doi.org/10.1097/00007632-199505000-00012.

[8] E. Nkenke, V. Weisbach, E. Winckler, P. Kessler, S. Schultze-Mosgau, J. Wiltfang, F. W. Neukam, Morbidity of harvesting of bone grafts from the iliac crest for preprosthetic augmentation procedures: a prospective study, Int. J. Oral Maxillofac. Surg. 33 (2004) 157–163, https://doi.org/10.1054/IJOM.2003.0465.

[9] N. Mardas, V. Chadha, N. Donos, Alveolar ridge preservation with guided bone regeneration and a synthetic bone substitute or a bovine-derived xenograft: a randomized, controlled clinical trial, Clin. Oral Implants Res. 21 (2010) 688–698, https://doi.org/10.1111/j.1600-0501.2010.01918.x.

[10] N. Kübler, J. Reuther, T. Kirchner, B. Priessnitz, W. Sebald, Osteoinductive, morphologic, and biomechanical properties of autolyzed, antigen-extracted, allogeneic human bone, J. Oral Maxillofac. Surg. 51 (1993) 1346–1357, https://doi.org/10.1016/S0278-2391(10)80141-7.

[11] C.J. Damien, J.R. Parsons, Bone graft and bone graft substitutes: a review of current technology and applications, J. Appl. Biomater.: Off. J. Soc. Biomater. 2 (1991) 187–208, https://doi.org/10.1002/jab.770020307.

[12] M. Bohner, L. Galea, N. Doebelin, Calcium phosphate bone graft substitutes: failures and hopes, J. Eur. Ceram. Soc. 32 (2012) 2663–2671, https://doi.org/10.1016/j.jeurceramsoc.2012.02.028.

[13] A. Kolk, J. Handschel, W. Drescher, D. Rothamel, F. Kloss, M. Blessmann, M. Heiland, K.D. Wolff, R. Smeets, Current trends and future perspectives of bone substitute materials - from space holders to innovative biomaterials, J. Cranio-Maxillofacial Surg. 40 (2012) 706–718, https://doi.org/10.1016/j.jcms.2012.01.002.

[14] C. Laurencin, Y. Khan, S.F. El-Amin, Bone graft substitutes, Expet Rev. Med. Dev. 3 (2006) 49–57.

[15] N. Passuti, G. Daculsi, J.M. Rogez, S. Martin, J. V Bainvel, Macroporous calcium phosphate ceramic performance in human spine fusion, Clin. Orthop. Relat. Res. 248 (1989) 169–176.

[16] M. Bohner, Resorbable biomaterials as bone graft substitutes, Mater. Today 13 (2010) 24–30, https://doi.org/10.1016/S1369-7021(10)70014-6.

[17] S. Yamada, D. Heymann, J.-M. Bouler, G. Daculsi, Osteoclastic resorption of calcium phosphate ceramics with different hydroxyapatite/β-tricalcium phosphate ratios, Biomaterials 18 (1997) 1037–1041, https://doi.org/10.1016/S0142-9612(97)00036-7.

[18] N. Kondo, A. Ogose, K. Tokunaga, T. Ito, K. Arai, N. Kudo, H. Inoue, H. Irie, N. Endo, Bone formation and resorption of highly purified β-tricalcium phosphate in the rat femoral condyle, Biomaterials 26 (2005) 5600–5608, https://doi.org/10.1016/J.BIOMATERIALS.2005.02.026.

[19] H. Yuan, H. Fernandes, P. Habibovic, J. de Boer, A.M. Barradas, A. de Ruiter, W. R. Walsh, C.A. van Blitterswijk, J.D. de Bruijn, Osteoinductive ceramics as a synthetic alternative to autologous bone grafting, in: Proceedings of the National Academy of Sciences of the United States of America vol. 107, United States National Academy of Sciences, 2010, pp. 13614–13619, https://doi.org/10.1073/pnas.1003600107.

[20] ISO 13175-3:2012 - Implants for surgery -, Calcium Phosphates - Part 3: Hydroxyapatite and Beta-Tricalcium Phosphate Bone Substitutes, International Organization for Standardization, 2012.

[21] M. Bohner, Bioresorbable ceramics, in: Fraser Buchanan (Ed.), Degradation Rate of Bioresorbable Materials : Prediction and Evaluation, Woodhead Publishing Ltd, 2008, pp. 95–114.

[22] J.-S. Sun, Y.-H. Tsuang, C.-J. Liao, H.-C. Liu, Y.-S. Hang, F.-H. Lin, The effects of calcium phosphate particles on the growth of osteoblasts, J. Biomed. Mater. Res. 37 (1997) 324–334, https://doi.org/10.1002/(SICI)1097-4636(19971205)37:3<324::AID-JBM3>3.0.

[23] T. Kitsugi, T. Yamamuro, T. Nakamura, S. Kotani, T. Kokubo, H. Takeuchi, Four calcium phosphate ceramics as bone substitutes for non-weight-bearing, Biomaterials 14 (1993) 216–224, https://doi.org/10.1016/0142-9612(93)90026-X.

[24] J.-S. Sun, Y.-C. Huang, F.-H. Lin, L.-T. Chen, The effect of sintered dicalcium pyrophosphate on osteoclast metabolism: an ultrastructural study, J. Biomed. Mater. Res. 64A (2003) 616–621, https://doi.org/10.1002/jbm.a.10439.

[25] P.S. Eggli, W. Müller, R.K. Schenk, Porous hydroxyapatite and tricalcium phosphate cylinders with two different pore size ranges implanted in the cancellous bone of rabbits. A comparative histomorphometric and histologic study of bony ingrowth and implant substitution, Clin. Orthop. Relat. Res. 232 (1988) 127–138.

[26] M. Descamps, J.C. Hornez, A. Leriche, Effects of powder stoichiometry on the sintering of β-tricalcium phosphate, J. Eur. Ceram. Soc. 27 (2007) 2401–2406, https://doi.org/10.1016/j.jeurceramsoc.2006.09.005.

[27] L. Hench, Biomaterials, Science 208 (1980) 826–831, https://doi.org/10.1126/SCIENCE.6246576.

[28] S. Yamada, D. Heymann, J.-M. Bouler, G. Daculsi, Osteoclastic resorption of calcium phosphate ceramics with different hydroxyapatite/β-tricalcium phosphate ratios, Biomaterials 18 (1997) 1037–1041, https://doi.org/10.1016/S0142-9612(97)00036-7.

[29] J.M. Bouler, P. Pilet, O. Gauthier, E. Verron, Biphasic calcium phosphate ceramics for bone reconstruction: a review of biological response, Acta Biomater. 53 (2017) 1–12, https://doi.org/10.1016/J.ACTBIO.2017.01.076.

[30] S.A. Redey, S. Razzouk, C. Rey, D. Bernache-Assollant, G. Leroy, M. Nardin, G. Cournot, Osteoclast adhesion and activity on synthetic hydroxyapatite, carbonated hydroxyapatite, and natural calcium carbonate: relationship to surface energies, J. Biomed. Mater. Res. 45 (1999) 140–147, https://doi.org/10.1002/(SICI)1097-4636 (199905)45:2<140::AID-JBM9>3.0.CO;2-I.

[31] D.O. Costa, P.D.H. Prowse, T. Chrones, S.M. Sims, D.W. Hamilton, A.S. Rizkalla, S. J. Dixon, The differential regulation of osteoblast and osteoclast activity bysurface topography of hydroxyapatite coatings, Biomaterials 34 (2013) 7215–7226, https://doi.org/10.1016/j.biomaterials.2013.06.014.

[32] A. Destainville, E. Champion, D. Bernache-Assollant, E. Laborde, Synthesis, characterization and thermal behavior of apatitic tricalcium phosphate, Mater. Chem. Phys. 80 (2003) 269–277, https://doi.org/10.1016/S0254-0584(02)00466-2.

[33] M. Descamps, O. Richart, P. Hardouin, J.C. Hornez, A. Leriche, Synthesis of Macroporous B -tricalcium Phosphate with Controlled Porous Architectural vol. 34, 2008, pp. 1131–1137, https://doi.org/10.1016/j.ceramint.2007.01.004.

[34] B. Le Gars Santoni, L. Niggli, G.A. Sblendorio, D.T.L. Alexander, C. Stähli, P. Bowen, N. Döbelin, M. Bohner, Chemically pure β-tricalcium phosphate powders: evidence of two crystal structures, J. Eur. Ceram. Soc. 41 (2021) 1683–1694, https://doi.org/10.1016/J.JEURCERAMSOC.2020.09.055.

[35] M. Gallo, B. Le Gars Santoni, T. Douillard, F. Zhang, L. Gremillard, S. Dolder, W. Hofstetter, S. Meille, M. Bohner, J. Chevalier, S. Tadier, Effect of grain orientation and magnesium doping on β-tricalcium phosphate resorption behavior, Acta Biomater. 89 (2019) 391–402, https://doi.org/10.1016/J.ACTBIO.2019.02.045.

[36] J. Bergmann, P. Friedel, R. Kleeberg, BGMN - a New Fundamental Parameters Based Rietveld Program for Laboratory X-Ray Sources, It's Use in Quantitative Analysis and Structure Investigations, International Union of Crystallography, 1998, pp. 5–8. Newsl 20.

[37] N. Doebelin, R. Kleeberg, Profex: a graphical user interface for the Rietveld refinement program BGMN, J. Appl. Crystallogr. 48 (2015) 1573–1580, https://doi.org/10.1107/S1600576715014685.

[38] ISO 13779-3:2018, Implants for Surgery - Hydroxyapatite - Part 3: Chemical Analysis and Characterization of Crystallinity Ratio and Phase Purity, International Organization for Standardization, 2018.

[39] Available on: <Http://imagej.nih.gov/ij/≥, NIH National Institute of Health, Image J, (n.d.).

[40] B. Dickens, L.W. Schroeder, W.E. Brown, Crystallographic studies of the role of Mg as a stabilizing impurity in β-Ca3(PO4)2. The crystal structure of pure β-Ca3(PO4)2, J. Solid State Chem. 10 (1974) 232–248, https://doi.org/10.1016/0022-4596(74)90030-9.

[41] N.C. Blumenthal, A.S. Posner, J.M. Holmes, Effect of preparation conditions on the properties and transformation of amorphous calcium phosphate, Mater. Res. Bull. 7 (1972) 1181–1189, https://doi.org/10.1016/0025-5408(72)90097-9.

[42] S. Raynaud, E. Champion, D. Bernache-Assollant, P. Thomas, Calcium phosphate apatites with variable Ca/P atomic ratio I. Synthesis, characterisation and thermal stability of powders, Biomaterials 23 (2002) 1065–1072, https://doi.org/10.1016/S0142-9612(01)00218-6.

[43] S. Raynaud, E. Champion, D. Bernache-Assollant, Calcium phosphate apatites with variable Ca/P atomic ratio II. Calcination and sintering, Biomaterials 23 (2002) 1073–1080, https://doi.org/10.1016/S0142-9612(01)00219-8.

[44] M. Descamps, L. Boilet, G. Moreau, A. Tricoteaux, J. Lu, A. Leriche, V. Lardot, F. Cambier, Processing and properties of biphasic calcium phosphates bioceramics obtained by pressureless sintering and hot isostatic pressing, J. Eur. Ceram. Soc. 33 (2013) 1263–1270, https://doi.org/10.1016/J.JEURCERAMSOC.2012.12.020.

[45] E. Champion, Sintering of calcium phosphate bioceramics, Acta Biomater. 9 (2013) 5855–5875, https://doi.org/10.1016/J.ACTBIO.2012.11.029.

[46] H.B. Lu, C.T. Campbell, D.J. Graham, B.D. Ratner, Surface characterization of hydroxyapatite and related calcium phosphates by XPS and TOF-SIMS, Anal. Chem. 72 (2000) 2886–2894, https://doi.org/10.1021/ac990812h.

[47] C.C. Chusuei, D.W. Goodman, M.J. Van Stipdonk, D.R. Justes, E.A. Schweikert, Calcium phosphate phase identification using XPS and Time-of-Flight Cluster SIMS, Anal. Chem. 71 (1999) 149–153, https://doi.org/10.1021/ac9806963.

[48] M. Kleine-Boymann, M. Rohnke, A. Henss, K. Peppler, J. Sann, J. Janek, Discrimination between biologically relevant calcium phosphate phases by surface-analytical techniques, Appl. Surf. Sci. 309 (2014) 27–32, https://doi.org/10.1016/J.APSUSC.2014.04.129.

[49] B. Mercer, F. Markland, C. Minkin, Contortrostatin, a homodimeric snake venom disintegrin, is a potent inhibitor of osteoclast attachment, J. Bone Miner. Res. 13 (1998) 409–414, https://doi.org/10.1359/jbmr.1998.13.3.409.

[50] T.L. Burgess, Y.-X. Qian, S. Kaufman, B.D. Ring, G. Van, C. Capparelli, M. Kelley, H. Hsu, W.J. Boyle, C.R. Dunstan, S. Hu, D.L. Lacey, D.L. Lacey, C.R. Dunstan, M. Kelley, M.-S. Chang, R. Luethy, H.Q. Nguyen, S. Wooden, L. Bennett, T. Boone, E.L. Timms, H.-L. Tan, M.J. Kelley, T. Burgess, R. Elliott, A. Colombero, G. Elliott,

S. Scully, The Ligand for Osteoprotegerin (OPGL) Directly Activates Mature Osteoclasts, Elsevier, Inc., 1999.
[51] W.J. Boyle, W.S. Simonet, D.L. Lacey, Osteoclast differentiation and activation, Nature 423 (2003) 337–342, https://doi.org/10.1038/nature01658.
[52] T.R. Arnett, D.W. Dempster, Effect of pH on bone resorption by rat osteoclasts in vitro, Endocrinology 119 (1986) 119–124, https://doi.org/10.1210/endo-119-1-119.
[53] T. Deguchi, M.H. Alanne, E. Fazeli, K.M. Fagerlund, P. Pennanen, P. Lehenkari, P. E. Hänninen, J. Peltonen, T. Näreoja, In vitro model of bone to facilitate measurement of adhesion forces and super-resolution imaging of osteoclasts, Sci. Rep. 6 (2016), 22585, https://doi.org/10.1038/srep22585.
[54] S.A. Clarke, J. Martin, J. Nelson, J.C. Hornez, M. Bohner, N. Dunne, F. Buchanan, Surrogate outcome measures of in vitro osteoclast resorption of β tricalcium phosphate, Adv. Healthcare Mater. 6 (2017), https://doi.org/10.1002/adhm.201600947.
[55] A.L. Wucherpfennig, Y.-P. Li, W.G. Stetler-Stevenson, A.E. Rosenberg, P. Stashenko, Expression of 92 kD type IV collagenase/gelatinase B in human osteoclasts, J. Bone Miner. Res. 9 (1994) 549–556, https://doi.org/10.1002/jbmr.5650090415.
[56] J. Brinkmann, T. Hefti, F. Schlottig, N.D. Spencer, H. Hall, Response of osteoclasts to titanium surfaces with increasing surface roughness: an in vitro study, Biointerphases 7 (2012) 34, https://doi.org/10.1007/s13758-012-0034-x.
[57] J. Costa-Rodrigues, A. Fernandes, M.A. Lopes, M.H. Fernandes, Hydroxyapatite surface roughness: complex modulation of the osteoclastogenesis of human precursor cells, Acta Biomater. 8 (2012) 1137–1145, https://doi.org/10.1016/J.ACTBIO.2011.11.032.
[58] Y. Maazouz, I. Rentsch, B. Lu, B. Le Gars Santoni, N. Doebelin, M. Bohner, In vitro measurement of the chemical changes occurring within β-tricalcium phosphate bone graft substitutes, Acta Biomater. 102 (2020) 440–457, https://doi.org/10.1016/j.actbio.2019.11.035.
[59] N. Döbelin, Y. Maazouz, R. Heuberger, M. Bohner, A.A. Armstrong, A.J. Wagoner Johnson, C. Wanner, A thermodynamic approach to surface modification of calcium phosphate implants by phosphate evaporation and condensation, J. Eur. Ceram. Soc. 40 (2020) 6095–6106, https://doi.org/10.1016/J.JEURCERAMSOC.2020.07.028.
[60] U. Gbureck, O. Grolms, J.E. Barralet, L.M. Grover, R. Thull, Mechanical activation and cement formation of β-tricalcium phosphate, Biomaterials 24 (2003) 4123–4131, https://doi.org/10.1016/S0142-9612(03)00283-7.
[61] R. Detsch, H. Mayr, G. Ziegler, Formation of osteoclast-like cells on HA and TCP ceramics, Acta Biomater. 4 (2008) 139–148, https://doi.org/10.1016/J.ACTBIO.2007.03.014.
[62] D.M. Lapierre, N. Tanabe, A. Pereverzev, M. Spencer, R.P.P. Shugg, S.J. Dixon, S. M. Sims, Lysophosphatidic Acid signals through multiple receptors in osteoclasts to elevate cytosolic calcium concentration, evoke retraction, and promote cell survival, J. Biol. Chem. 285 (2010) 25792–25801, https://doi.org/10.1074/JBC.M110.109322.
[63] F. Pascaretti-Grizon, G. Mabilleau, M.F. Basle, D. Chappard, Measurement by vertical scanning profilometry of resorption volume and lacunae depth caused by osteoclasts on dentine slices, J. Microsc. 241 (2011) 147–152, https://doi.org/10.1111/j.1365-2818.2010.03410.x.
[64] T. Okuda, K. Ioku, I. Yonezawa, H. Minagi, G. Kawachi, Y. Gonda, H. Murayama, Y. Shibata, S. Minami, S. Kamihira, H. Kurosawa, T. Ikeda, The effect of the microstructure of β-tricalcium phosphate on the metabolism of subsequently formed bone tissue, Biomaterials 28 (2007) 2612–2621, https://doi.org/10.1016/J.BIOMATERIALS.2007.01.040.
[65] N.L. Davison, B. ten Harkel, T. Schoenmaker, X. Luo, H. Yuan, V. Everts, F. Barrère-de Groot, J.D. de Bruijn, Osteoclast resorption of beta-tricalcium phosphate controlled by surface architecture, Biomaterials 35 (2014) 7441–7451, https://doi.org/10.1016/J.BIOMATERIALS.2014.05.048.
[66] T.J. Webster, C. Ergun, R.H. Doremus, R.W. Siegel, R. Bizios, Enhanced osteoclast-like cell functions on nanophase ceramics, Biomaterials 22 (2001) 1327–1333, https://doi.org/10.1016/S0142-9612(00)00285-4.
[67] L.M. Grover, A.J. Wright, U. Gbureck, A. Bolarinwa, J. Song, Y. Liu, D.F. Farrar, G. Howling, J. Rose, J.E. Barralet, The effect of amorphous pyrophosphate on calcium phosphate cement resorption and bone generation, Biomaterials 34 (2013) 6631–6637, https://doi.org/10.1016/J.BIOMATERIALS.2013.05.001.
[68] J.-S. Sun, Y.-C. Huang, Y.-H. Tsuang, L.-T. Chen, F.-H. Lin, Sintered dicalcium pyrophosphate increases bone mass in ovariectomized rats, J. Biomed. Mater. Res. 59 (2002) 246–253, https://doi.org/10.1002/jbm.1238.